PNAS RESEARCH ARTICLE | IMMUNOLOGY AND INFLAMMATION

Structural insights reveal interplay between LAG-3 homodimerization, ligand binding, and function

John L. Silberstein[a,b,1], Jasper Du[c,1], Kun-Wei Chan[d], Jessica A. Frank[b], Irimpan I. Mathews[e], Yong Bin Kim[b,f], Jia You[c], Qiao Lu[c], Jia Liu[c], Elliot A. Philips[d], Phillip Liu[b,g], Eric Rao[c], Daniel Fernandez[h], Grayson E. Rodriguez[a,i], Xiang-Peng Kong[d], Jun Wang[c,j,2], and Jennifer R. Cochran[a,b,f,2]

Edited by Michael Dustin, University of Oxford, Oxford, United Kingdom; received June 27, 2023; accepted January 2, 2024

Lymphocyte activation gene-3 (LAG-3) is an inhibitory receptor expressed on activated T cells and an emerging immunotherapy target. Domain 1 (D1) of LAG-3, which has been purported to directly interact with major histocompatibility complex class II (MHCII) and fibrinogen-like protein 1 (FGL1), has been the major focus for the development of therapeutic antibodies that inhibit LAG-3 receptor-ligand interactions and restore T cell function. Here, we present a high-resolution structure of glycosylated mouse LAG-3 ectodomain, identifying that cis-homodimerization, mediated through a network of hydrophobic residues within domain 2 (D2), is critically required for LAG-3 function. Additionally, we found a previously unidentified key protein-glycan interaction in the dimer interface that affects the spatial orientation of the neighboring D1 domain. Mutation of LAG-3 D2 residues reduced dimer formation, dramatically abolished LAG-3 binding to both MHCII and FGL1 ligands, and consequentially inhibited the role of LAG-3 in suppressing T cell responses. Intriguingly, we showed that antibodies directed against D1, D2, and D3 domains are all capable of blocking LAG-3 dimer formation and MHCII and FGL-1 ligand binding, suggesting a potential allosteric model of LAG-3 function tightly regulated by dimerization. Furthermore, our work reveals unique epitopes, in addition to D1, that can be targeted for immunotherapy of cancer and other human diseases.

LAG-3 | immune checkpoint | dimerization | cancer immunotherapy | structural biology

Immune checkpoint receptors are crucial in regulating the immune response and maintaining self-tolerance and are key players in the immune evasion mechanisms used by cancer cells, enabling them to escape immune recognition and attack (1). The programmed cell death protein 1 (PD-1) and cytotoxic T lymphocyte-associated antigen 4 are the most well-known checkpoint receptors, with targeted antibody antagonists against them having greatly revolutionized cancer therapy (1). Like PD-1, LAG-3 (Lymphocyte activation gene-3) is a checkpoint receptor that becomes up-regulated upon T cell activation and negatively regulates the proliferation, activation, effector function, and homeostasis of both CD8+ and CD4+ T cells, as shown in LAG-3 overexpression and knockout studies (2, 3). LAG-3 represents an "exhaustion" marker for CD8+ T cells and is usually co-expressed with PD-1 in response to repetitive antigen stimulation in chronic viral infections and cancers (4, 5). Despite positive effects of anti-LAG-3 antibodies in clinical trials for the treatment of cancer (6), the mechanism by which LAG-3 functions remains poorly understood.

LAG-3 is a type I transmembrane protein with four extracellular immunoglobulin (Ig)-like domains (D1 to D4). Major histocompatibility class II (MHCII) was first identified as a ligand for LAG-3 (7), based on the high homology of LAG-3's D1 to D4 domains to that of CD4, a glycoprotein that serves as a co-receptor for the T cell receptor. Fibrinogen-like protein 1 (FGL1) has more recently been identified as an emerging new checkpoint ligand of LAG-3 (8). The D1 domain of LAG-3 is purported to be the major binding domain that interacts with MHCII and FGL1. MHCII is thought to bind to a long 30 amino acid loop (loop 1) on D1; deletion of this loop results in diminished MHCII binding (9). Deletion of the D2 domain also results in reduced MHCII binding; however, the mechanism by which D2 interacts with MHCII is not characterized (9). In contrast, FGL1 is purported to bind a second loop on D1 (Loop 2), which is located on an opposite face of the D1 domain from the MHCII binding site (10). Like MHCII, FGL1 has also been shown to require the LAG-3 D2 domain for maximal binding to LAG-3 (8).

Upon ligand binding, LAG-3 negatively regulates T cells through its intracellular domain (ICD) (3, 11). Unlike the cytoplasmic tails of PD-1 and other checkpoint receptors which regulate T cell function through an immunoreceptor tyrosine-based inhibition motif, LAG-3

Significance

T cell activation is tightly regulated by activating and inhibitory receptors. One of these inhibitory receptors, Lymphocyte activation gene-3 (LAG-3), is currently being targeted in oncology clinical trials to enhance anti-tumor immunity. However, the mechanism by which LAG-3 inhibits T cells is poorly understood. We show that LAG-3 homodimerizes on the cell surface and that this homodimerization is crucial for positioning LAG-3 in the proper orientation to bind to its ligands and drive LAG-3 inhibitory function. We also show that preventing LAG-3 homodimerization by either mutation or antibody binding, even at epitopes distinct from the dimerization interface, can rescue T cells from LAG-3-mediated inhibition, providing an opportunity to utilize LAG-3 dimer disruption in cancer immunotherapy.

This article is a PNAS Direct Submission.

[1]J.L.S. and J.D. contributed equally to this work.

[2]To whom correspondence may be addressed. Email: jun.wang@nyulangone.org or cochran1@stanford.edu.

This article contains supporting information online at https://www.pnas.org/lookup/suppl/doi:10.1073/pnas.2310866121/-/DCSupplemental.

Published March 14, 2024.

is thought to deliver its inhibitory signal through an FxxL motif and a tandem glutamic acid-proline negatively charged repeat (12). Recent evidence suggests that the negatively charged portion of the LAG-3 cytoplasmic tail is crucial in blocking the association of activating kinases with the cytoplasmic tails of the CD4 and CD8 co-receptors, rather than blocking an extracellular interaction between CD4 and MHCII (11).

The importance of the MHCII/LAG-3 interaction to LAG-3's immunosuppressive function remains unclear, as several monoclonal antibodies (mAbs) that do not bind to the D1 domain can promote T cell function (8, 10, 13). For example, C9B7W, a mAb against the murine LAG-3 D2 domain, enhances T cell proliferation and effector functions in cell culture and animal tumor models (8). Yet, depending on the model system used, this antibody has variable ability to block LAG-3 binding to MHCII, ranging from complete inability to partial or full ability (13–17). The effect of C9B7W on T cells is similar, if not identical, to that produced by LAG-3 genetic deficiency (18, 19). In another study, an anti-LAG-3 mAb called F7, which does not block MHCII binding, could still rescue T cells from LAG-3-mediated inhibition and stimulate T cell activation (10). Moreover, LAG-3 has been proposed to inhibit T cell function in the absence of MHCII ligation (11) and can suppress the function of CD8+ T cells and natural killer (NK) cells which do not primarily interact with MHCII (20), highlighting that the immunological functions and molecular mechanisms mediated by LAG-3 are complex and not fully understood.

Early reports suggested that LAG-3 dimerizes through its first, most membrane distal domain (D1), which is involved in ligand binding (9, 21). During the course of our work, Ming et al. showed that partially deglycosylated LAG-3 extracellular domain (ECD) dimerizes through the D2 domain; however, the relevance of this cis-homodimerization in LAG-3 function remains unknown (10). Here, we present the structure of full-length glycosylated mouse LAG-3 ECD and validate cis-homodimerization through the D2 domain. Importantly, we show that the D2 dimerization interface and orientation of the flanking domains are mediated by a key protein–glycan interaction in addition to a network of evolutionarily conserved protein–protein and protein–glycan interactions. Disruption of these LAG-3 cis-homodimers at the cell surface by site-directed mutagenesis abrogates the ability of LAG-3 to bind to its ligands MHCII and FGL1. Further, our data show that LAG-3 requires cis-homodimerization for its T cell suppressive activity. We finally demonstrate that multiple LAG-3-specific antibodies, including the commonly used LAG-3 inhibitor C9B7W, are capable of disrupting LAG-3 dimerization. Together, our data reveal that glycosylation and cis-homodimerization play key roles in LAG-3 function.

Results

Structure of Glycosylated Mouse LAG-3 ECD. To better understand the native structure of LAG-3, we performed negative stain electron microscopy (EM) with a recombinant, soluble form of glycosylated mouse LAG-3 D1 to D4 ECD (Fig. 1*A*). Using this approach, we were able to visualize homodimerization of two LAG-3 monomers; however, the resolution was not sufficient to determine the key intermolecular forces mediating this dimer formation. In parallel, we worked to crystallize the glycosylated mouse LAG-3 D1 to D4 ECD and to solve the structure by X-ray crystallography. Due to the flexibility of the LAG-3 protein, inherent diffraction issues, and a lack of similar proteins in the PDB at the time these activities were carried out, our early attempts were unsuccessful. Ultimately, we screened 3,063 crystals to obtain 1.3Tb of diffraction data. Upon the release of the AlphaFold Protein Structure Database (22, 23), we were able to use a combination of three datasets and the AlphaFold-predicted monomeric structure of human LAG-3 D1 to D3 ECD for molecular replacement and structural solution (24). One chain of the LAG-3 homodimeric structure can be visualized from D1 to D4, while flexibility in the protein precluded us from resolving D4 in the opposite chain (*SI Appendix*, Fig. S1*A*). Our structure of the mouse LAG-3 ECD is refined to 3.78 Å resolution (Fig. 1*B* and *SI Appendix*, Fig. S1*A*).

Based on our structure, LAG-3's predicted height from the cell surface appears to be similar to that of the CD4:MHCII:TCR complex (*SI Appendix*, Fig. S1 *A* and *B*) (25, 26). LAG-3 D1 consists of an Ig-like V-type domain, followed by three Ig-like C2-type domains that comprise D2 through D4, in the same orientation as CD4 (*SI Appendix*, Fig. S1 *A* and *B*). Compared to the CD4 apo structure, LAG-3 D1 is rotated outward approximately 26° (*SI Appendix*, Fig. S1*C*). This rotation may allow additional space for the 30 amino acid Loop 1 in LAG-3. In our structural model, loop 1 could not be completely built due to its long, flexible nature; however, a portion of the human LAG-3 loop, in complex with an antibody fragment, has recently been resolved (PDB 7UM3) (19).

Although previous reports have suggested that LAG-3 dimerizes through the D1 domain (9, 21), our structure characterized glycosylated LAG-3 dimerization through D2 (Fig. 1 *A* and *B*), consistent with a recent report of partially deglycosylated LAG-3 protein (10). A small shift in molecular weight was observed as analyzed by sodium dodecyl-sulfate polyacrylamide gel electrophoresis (SDS-PAGE) when LAG-3 was expressed in Expi293F GnTI- cells to remove complex N-linked glycans (Fig. 1*C*). When this protein was further processed by the endoglycosidase EndoHf to remove high-mannose N-linked oligosaccharides, we observed an apparent ~10 kDa shift in LAG-3 protein size by SDS-PAGE (Fig. 1*C*). With endoglycosidase F1-treated glycans, the D1 and D2 domains of mouse LAG-3 and the subsequent crystallographic dimer present with an angle of ~70° between the D2 monomer units (PDB 7TZE, Fig. 1*D*) (10). By using LAG-3 without any modified or truncated glycans in our study, we were able to visualize two unique, bulky N-linked glycans significantly contributing to the dimerization interface in a more upright orientation, with a ~35° angle between D2 domains (Fig. 1*E*). Furthermore, when comparing our structure to the partially deglycosylated human LAG-3 ECD (PDB 7TZG, Fig. 1*F*), we observed a larger angle between our mouse LAG-3 D2 domains (23.9° vs. 34.6°) as well as an outward rotation of the human LAG-3 D4 domain (*SI Appendix*, Fig. S1*D*). These differences may potentially be explained by a number of variances, including glycosylation state, crystal packing, mutation of residue M171 to isoleucine in the human LAG-3 protein, inherent species differences between human and mouse LAG-3, or the presence of a D4-binding scFv antibody fragment co-complexed with human LAG-3 in the prior structure (10). Given its flexibility, LAG-3 may also exist in multiple conformations on the cell surface and interconvert between the different states that have been observed in these static structures (Fig. 1 *D*–*F*).

Our murine LAG-3 structure superimposes with the previous murine LAG-3 D1D2 structure (PDB 7TZE) with a rmsd of 1.4 Å for one monomer and 1.1 Å for the other monomer. While the D1 domains show variability between the structures (rmsd 1.1 Å to 1.7 Å), the D2 domains overlap well between the monomers in all structures (rmsd 0.6 Å to 0.8 Å). We further identified an N-linked glycan on N184 that was bridged by residue R192 on the opposite chain of the LAG-3 dimer (Fig. 2*A* and *SI Appendix*,

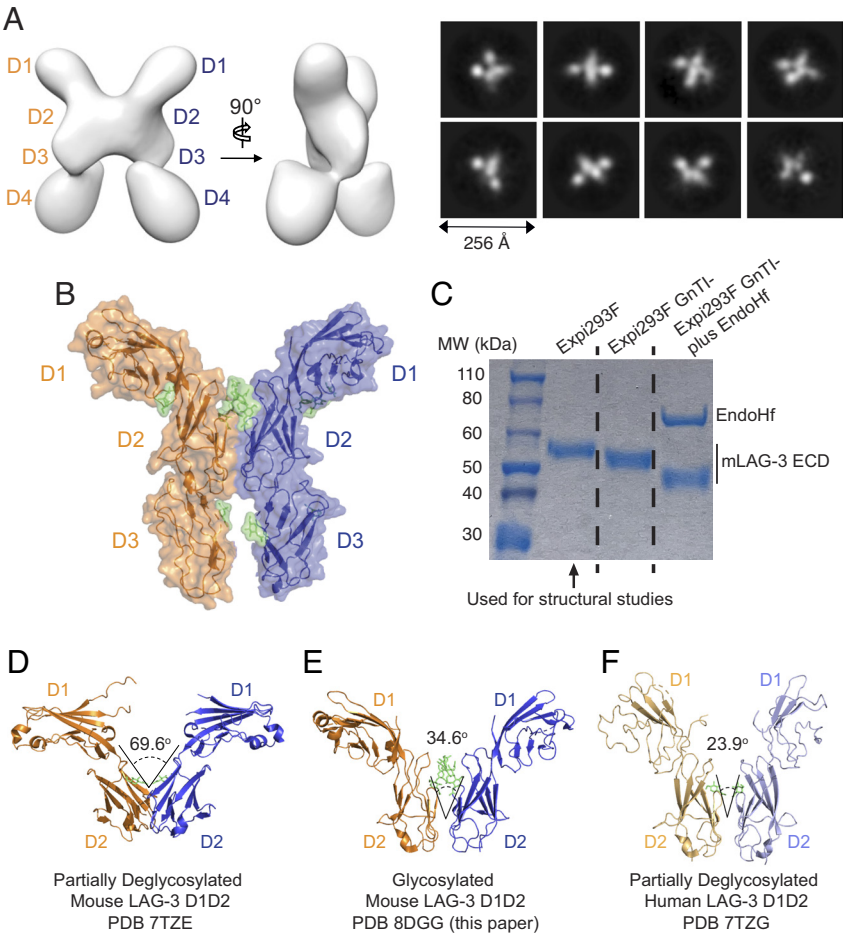

Fig. 1. Structure of the glycosylated LAG-3 dimer. (*A*) Negative stain EM 3D reconstruction map model of LAG-3 dimer and selected reference-free 2D class averages. Four ECDs (D1 to D4) were labeled on the corresponding positions in both LAG-3 molecules of the dimer map model. (*B*) Surface representation of domains 1 to 3 in the dimeric LAG-3 structure. Glycans are shown in green. (*C*) SDS-PAGE of mouse LAG-3 ECD expressed and purified from Expi293F cells, Expi293F GnTI- cells, and Expi293F GnTI- cells, followed by EndoHf treatment. The predicted molecular weights of the LAG-3 ECD and EndoHf are 46.2 kDa and 70 kDa, respectively. The shift in molecular weight between glycosylated and deglycosylated mouse LAG-3 represents approximately 10 kDa of N-linked glycans. Glycosylated protein from Expi293F cells was used for crystal structure determination. (*D–F*) Cartoon structures of the partially deglycosylated mouse LAG-3 domains 1 and 2 (PDB 7TZE), the glycosylated mouse LAG-3 domains 1 and 2 (PDB 8DGG; this paper), and the partially deglycosylated human LAG-3 domains 1 and 2 (PDB 7TZG). Glycans are shown in green. The glycan-protein interaction at the *Top* of the D2 dimer interface brings two monomers together and increases the buried surface area from 440 Å^2 in the partially deglycosylated mouse LAG-3 structure to 511 Å^2 in the glycosylated mouse LAG-3 structure.

Fig. S2 *A* and *B*). Directly below this glycan–protein interface, we observed an extensive network of hydrophobic protein–protein interactions (Fig. 2*B*). These evolutionarily conserved hydrophobic interface residues contribute much of the buried surface area to the D2-mediated cis-homodimerization (Fig. 2*B* and *SI Appendix*, Fig. S3 *A* and *B*). We were able to visualize protein–protein contacts between 7 hydrophobic residues from the D2 domain of each monomer, including W180, L182, F214, A216, F219, L221, and P223 (Fig. 2*B* and *SI Appendix*, Fig. S3*A*). These interactions allow the cis-homodimer to form in the absence of glycans (Fig. 1*D*), with a buried surface area observed in the previous structures of mouse and human LAG-3 D2 of approximately 440 and 438 Å^2, respectively (10). In contrast, fully glycosylated LAG-3 D2 buries 511 Å^2 of surface area, potentially due to stabilization from the bulky glycan–protein interaction at positions N184 and R192 (Fig. 1*E*).

LAG-3 Dimerizes in a Cellular Context. While our studies confirm that recombinant, soluble LAG-3 D1 to D4 ECD can exist as a dimer, it is unclear whether full-length LAG-3, including the transmembrane and ICDs, also dimerizes. Flow cytometry-based Förster resonance energy transfer (flow-FRET) assays have been widely utilized for live cell detection of proximal protein associations at distances <100 Å and was thus used to assess LAG-3 dimerization (3, 7, 11, 27). To analyze LAG-3 on the cell surface, Expi293F cells were co-transfected with both LAG-3 cyan fluorescent protein (CFP) and LAG-3 yellow fluorescent protein (YFP) and compared against other fusion proteins for detection of FRET (Fig. 2*C* and *SI Appendix*, Fig. S4). Indeed, both mouse and human LAG-3 showed a positive FRET signal, suggesting dimerization on the surface of cells (Fig. 2*D*). As a negative control, mouse LAG-3 CFP was co-transfected with human CD80 YFP (hCD80^{YFP}), which had no detectable FRET signal, suggesting no association between these two receptors, while hCD80^{CFP}/hCD80^{YFP} (a known homodimer) showed positive FRET signal (Fig. 2*D*). We saw reduced FRET positivity (~50%) for the homodimers compared to an intracellular genetic fusion of CFP with YFP, which is potentially attributable to homodimer CFP/CFP or YFP/YFP pairings (Fig. 2*D*).

We next introduced a single point mutation within the D2 dimerization interface to assess whether dimer formation could be disrupted and measured by FRET. Mutation of W180, one of the most conserved residues in the D2 dimerization interface (*SI Appendix*, Fig. S3*B*), to aspartic acid in LAG-3 donor (CFP-tagged) and acceptor

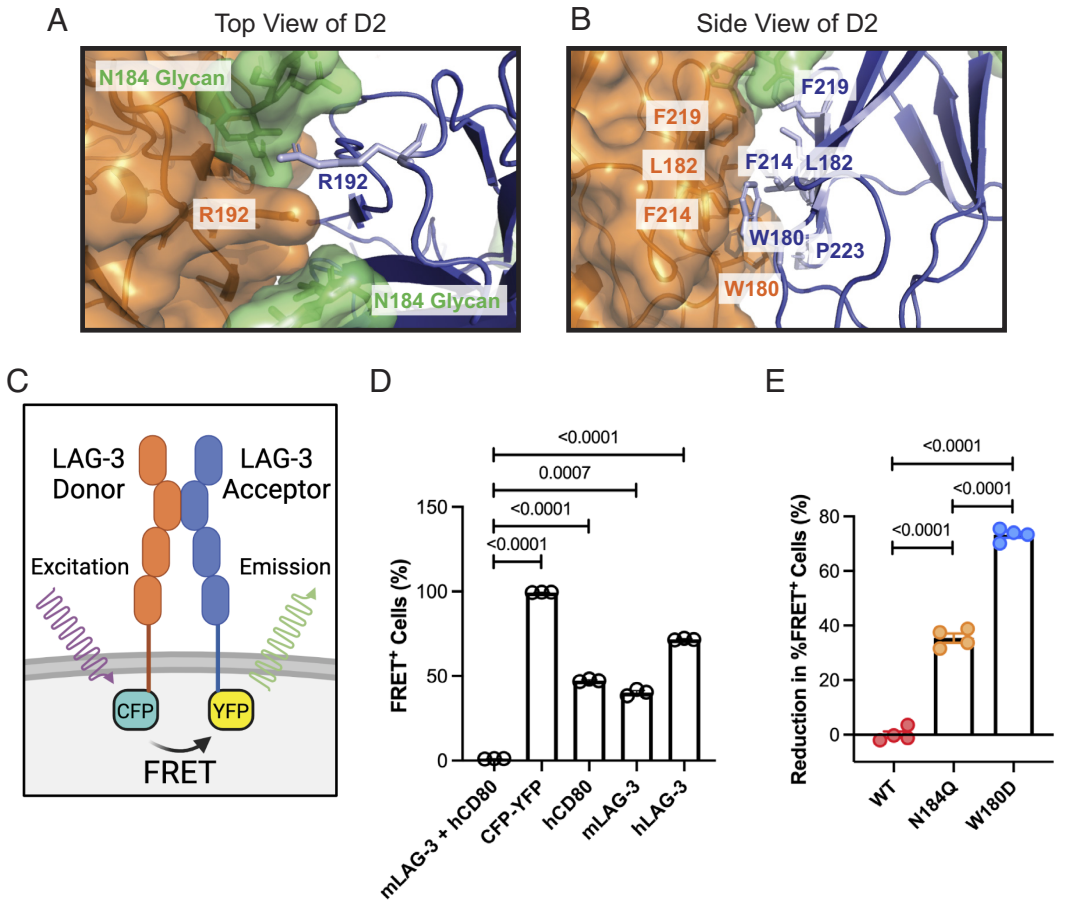

Fig. 2. Glycosylation and homodimerization at the D2 dimer interface. (*A*) Contact residues in the D2 dimer interface are shown. R192 and the negatively charged glycan on N184 can be visualized in the *Top* view. (*B*) The side view shows an extensive network of hydrophobic interacting residues. (*C*) Graphical representation of flow-FRET experiments using two-chain, two-plasmid system with Expi293F cells. (*D*) Flow-FRET data from Expi293F cells comparing CFP-YFP fused by a linker to double transfections of mLAG-3^{CFP}/hCD80^{YFP}, hCD80^{CFP}/hCD80^{YFP} (known homodimer), mLAG-3^{CFP}/mLAG-3^{YFP}, and hLAG-3^{CFP}/hLAG-3^{YFP}. (*E*) Flow-FRET data showing the effect of the N184Q and W180D mutations on LAG-3 dimerization. Reduction in %FRET^{+} cells was calculated relative to WT. The data in (*D*) and (*E*) are presented as the mean ± SEM and are representative of at least two independent experiments. All statistics were determined by Student's *t* test with *P* values noted in the figure.

(YFP-tagged) proteins led to a significant reduction in FRET signal, indicating a reduction in dimerization (Fig. 2*E* and *SI Appendix*, Fig. S5*A*). For the chains to repel each other, a charged residue was required, as mutation to a minimal hydrophobic residue using W180A had no effect on LAG-3 FRET signal (*SI Appendix*, Fig. S5 *B* and *C*). To probe the importance of the glycan–protein interaction in dimer formation, an N184Q mutation was also tested and reduced FRET, albeit weaker than that of W180D mutation (Fig. 2*E* and *SI Appendix*, Fig. S5*A*).

Disruption of LAG-3 Cis-Homodimerization Affects LAG-3 Ligand Binding and Function. We next sought to determine whether a reduction in dimerization would affect LAG-3 ligand binding and T cell function. Wild-type LAG-3 and the dimerization-affecting mutants N184Q and W180D were stably expressed in the CD4^{+} I-A^{k}-HEL$_{50\text{-}62}$ reactive T cell hybridoma, 3A9, and were found to be present on the cell surface at similar levels (*SI Appendix*, Fig. S6*A*). We then used a tetrameric form of MHCII (I-A^{b}) covalently bound to ovalbumin peptide (OVA$_{323\text{-}339}$) to selectively stain 3A9 cells, which bear a non-cognate TCR, in a LAG-3-dependent manner. The dimer-disrupting mutation W180D completely nullified LAG-3-dependent 3A9 binding to pMHCII tetramer as well as FGL1, whereas the N184Q mutant reduced LAG-3-dependent binding to pMHCII tetramer and FGL1 to a lesser extent than W180D (Fig. 3 *A* and *B*). We next evaluated whether these LAG-3 mutants could affect LAG-3 function on T cells. When stimulated by I-A^{k}-HEL$_{50\text{-}62}$ cognate peptide, both N184Q and W180D relieved LAG-3 inhibition, as observed by elevated IL-2 production compared to the vector-transduced 3A9 control, with the W180D mutant resulting in a greater effect (Fig. 3*C*). To further confirm these results and the impact of N184Q and W180D on LAG-3 function, we repeated these experiments with the DO11.10 T cell hybridoma which recognizes OVA$_{323\text{-}339}$ presented by I-A^{d} (expressed on the surface of LK35.2 B cells). Consistent with our 3A9 findings, both the dimerization-disrupting mutants N184Q and W180D resulted in loss of LAG-3 binding to ligands and LAG-3 inhibitory function in DO11.10 T cells (Fig. 3 *D*–*F* and *SI Appendix*, Fig. S6*B*). Again, W180D had a more pronounced effect on LAG-3 binding and function when compared to the N184Q mutation. These data indicate that cis-homodimerization is critical to LAG-3's ability to bind MHCII and FGL1 ligands and mediate T cell suppression.

Mouse LAG-3 D2 Antibody C9B7W Binds at the Dimer Interface and Affects LAG-3 Function. With a newfound interest in D2 cis-dimerization and its function in LAG-3 biology, we aimed to identify specific antibodies that can directly engage with the dimerization interface. We first tested a commonly used mouse

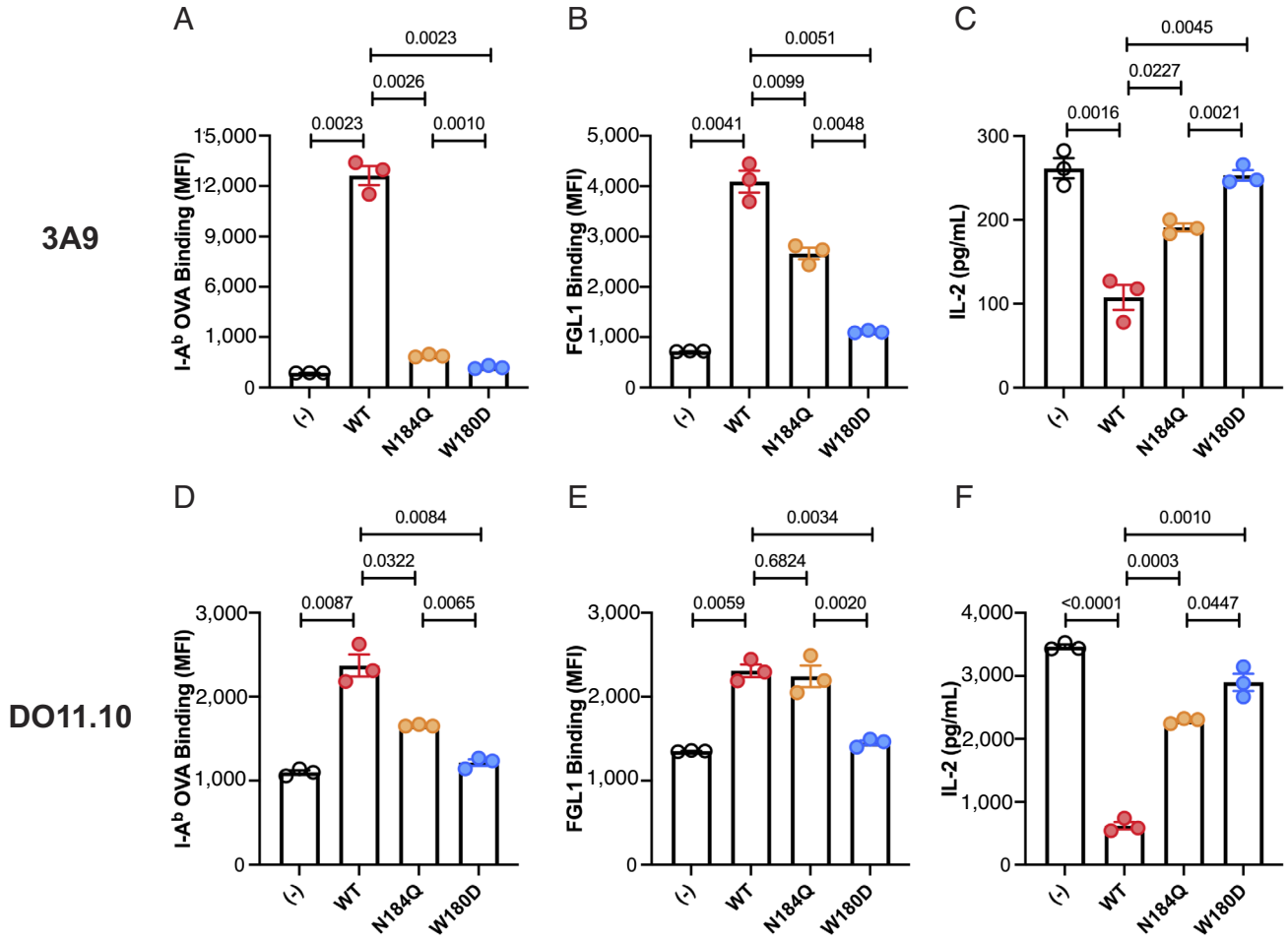

Fig. 3. Dimerization has a critical role in LAG-3 function. 3A9 cells were stably transduced with LAG-3 variants and tested for their ability to bind (*A*) non-cognate pMHCII tetramer and (*B*) FGL1 dimer. (*C*) LAG-3 expressing 3A9 cells co-cultured with 293T cells expressing cognate peptide-MHCII to evaluate LAG-3 function. LAG-3-expressing DO11.10 cells were also tested for their ability to bind (*D*) non-cognate pMHCII tetramer and (*E*) FGL1 dimer. (*F*) LAG-3-expressing DO11.10 cells were co-cultured with LK35.2 B cells pulsed with cognate peptide to evaluate LAG-3 function. Empty vector transduced T cells are represented by (−). The data are presented as the mean ± SEM and are representative of at least two independent experiments. All statistics were determined by Student's *t* test with *P* values noted in the figure.

LAG-3 D2 antibody, C9B7W, which has been used extensively as a functional LAG-3 inhibitor for both in vitro and in vivo studies (8, 12, 13, 16, 18). C9B7W was reported to block the FGL1/LAG-3 interaction (8) but had no or weak capacity to block LAG-3's interaction with MHCII, in the context of an MHCII-Fc fusion protein or MHCII expressed on the cell surface (12–15). However, the debate has continued with recent studies showing that high concentrations of C9B7W could block, at least in part, the MHCII/LAG-3 interaction when tested by MHCII tetramer (16, 17). Given that this antibody does not bind to the D1 domain (13), including the MHCII-interacting Loop 1 region as well as the FGL1-interacting Loop 2 region (10), the detailed characterization of the C9B7W binding epitope will therefore provide critical information with regard to how this D2-targeted antibody works in inhibiting LAG-3 function.

Guided by our structure of mouse LAG-3, we performed fine epitope mapping of the C9B7W antibody by yeast surface display (28). Due to poor expression levels of mouse LAG-3 D1 to D4 ECD on the yeast cell surface, we instead created a set of 95 individual alanine mutations of solvent-accessible residues on LAG-3 D1D2 domains, with equal distribution throughout the protein surface (*SI Appendix*, Fig. S7 *A* and *B*). We displayed the mutant LAG-3 D1D2 proteins, along with the wild-type LAG-3 D1D2 domains, individually on the surface of yeast, fused at the C-terminus to the Aga2p mating protein (29). Using flow cytometry and fluorescent antibody staining, we then measured LAG-3 variant protein expression levels using an antibody against a C-terminal c-Myc tag and binding to C9B7W antibody (*SI Appendix*, Fig. S7 *A* and *B*). A hybridoma-generated Loop 1 antibody (M2-6-8) was used as a control to further normalize for protein expression levels at the N-terminus of LAG-3. With this method of fine epitope mapping, we found that the C9B7W antibody binds directly at the LAG-3 D2 dimer interface (Fig. 4*A*). Specifically, LAG-3 mutations of W180, N209, and F214 to alanine resulted in reduced binding signal for C9B7W (Fig. 4*A*). Along with our FRET and T cell assay data, recognition of W180 by C9B7W further highlights the functional relevance of this amino acid in LAG-3 biology.

We then tested whether the C9B7W antibody was capable of disrupting LAG-3 dimerization, building on our initial negative stain EM studies (Fig. 1*A*). A Fab fragment of C9B7W was prepared and incubated with mouse LAG-3 in a 1:1 ratio, and the resulting complex was placed onto grids for negative stain EM. While mouse LAG-3 devoid of binding partners formed dimers on the grid (Fig. 1*A*), mouse LAG-3 complexed with C9B7W only presented in monomeric form (Fig. 4*B*). We used our structure, negative stain EM, and epitope mapping data to reconstruct a 3D model of C9B7W bound to mouse LAG-3 (Fig. 4*B*). We

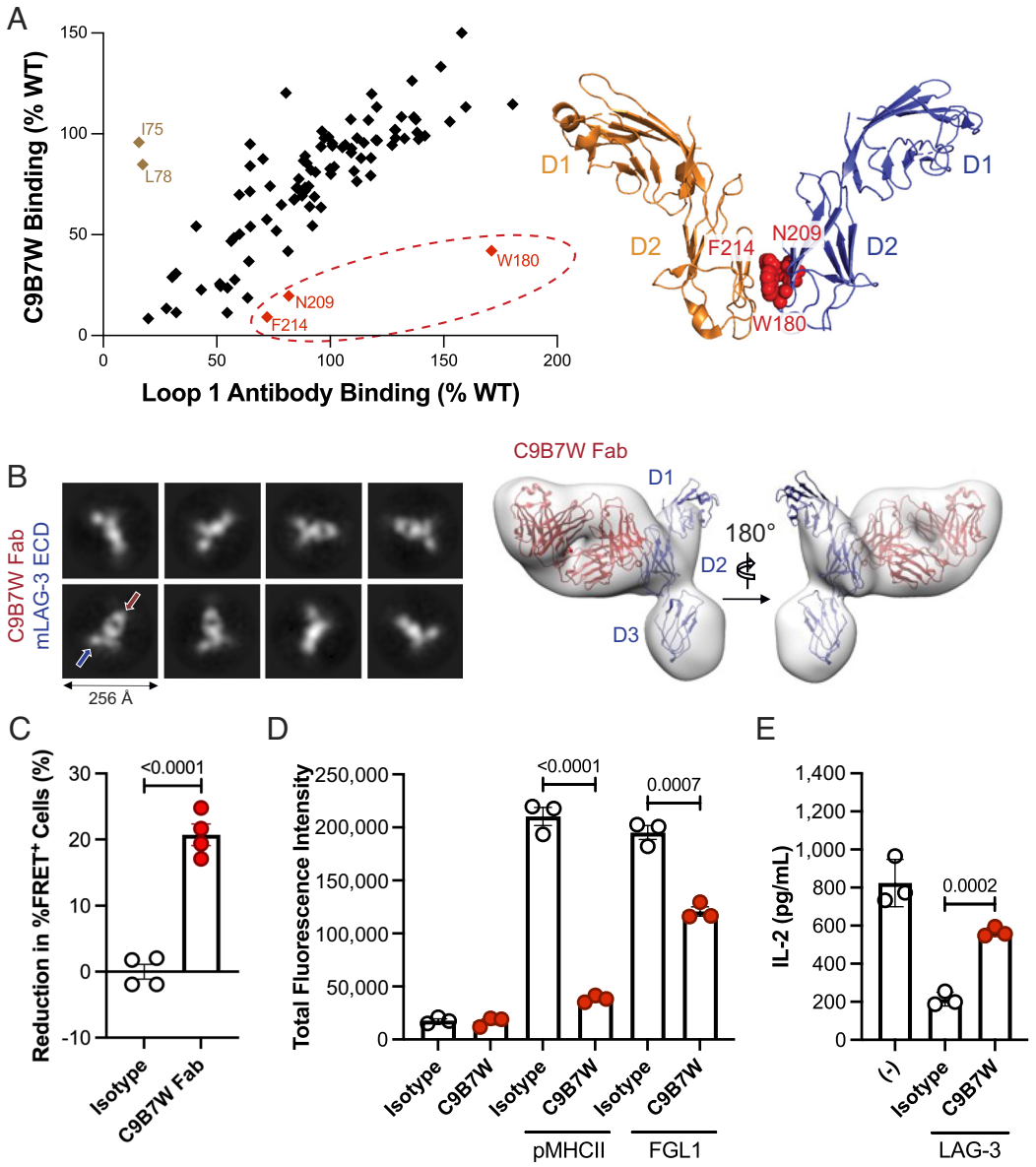

Fig. 4. C9B7W binds to D2 dimerization interface, disrupts LAG-3 dimerization, and blocks ligand binding. (*A*) Fine epitope mapping of C9B7W by yeast surface display reveals a binding epitope at the dimer interface of LAG-3. LAG-3 residues important for C9B7W binding (W180, N209, F214) are displayed as red spheres on the LAG-3 dimer. (*B*) Negative stain EM showing selected 2D class averages and the 3D map model of the C9B7W Fab with mouse LAG-3. (*C*) Flow-FRET data showing the effect of C9B7W Fab on LAG-3 dimerization. Reduction in %FRET^{+} cells was calculated relative to the isotype. (*D*) LAG-3 CAR assay to evaluate LAG-3 ligand engagement in the presence of C9B7W. Jurkat cells stably expressing a NFκB-GFP reporter and a LAG-3 CAR were co-cultured with 293T cells stably expressing pMHCII or transmembrane-fused FGL1. (*E*) IL-2 secretion to measure LAG-3-dependent T cell inhibition in the presence or absence of C9B7W. DO11.10 cells expressing LAG-3 were co-cultured with LK35.2 cells pulsed with cognate peptide. Empty vector transduced T cells are represented by (−). The data in (*C*) and (*D*) are presented as the mean ± SEM and are representative of at least two independent experiments. All statistics were determined by Student's *t* test with *P* values noted in the figure.

further evaluated whether the C9B7W Fab could disrupt full length LAG-3 dimerization by flow-FRET. Indeed, reduced FRET was observed upon incubation of C9B7W with cells expressing LAG-3 CFP and LAG-3 YFP (Fig. 4*C*), while no reduction in FRET was observed upon incubation of C9B7W with cells expressing CD80 CFP and CD80 YFP (*SI Appendix*, Fig. S8 *A* and *D*). These data, combined with our finding that the dimer-disrupting mutant W180D is incapable of binding to pMHCII, support the hypothesis that C9B7W may function through affecting LAG-3 dimerization.

Given the current debate surrounding the ability of C9B7W to affect LAG-3 ligand–receptor interactions, it is important to draw conclusions from a more physiological cell-cell interaction assay that excludes the use of recombinant proteins. We therefore built a sensitive LAG-3 chimeric antigen receptor (CAR) assay which generates a strong signal upon LAG-3 ligand engagement. In this assay, 293T cells stably expressing pMHCII are co-cultured with Jurkat cells stably expressing an NFκB-GFP reporter and a LAG-3 CAR that consists of the LAG-3 ECD and CD28/41BB/CD3z ICD (*SI Appendix*, Fig. S9 *A* and *B*). Upon the engagement of either MHCII (I-A^{k}-$HEL_{50\text{-}62}$) or FGL1 (fused with a transmembrane-domain) by the LAG-3 CAR, we observed strong T cell activation as indicated by the NFκB-dependent GFP reporter signal (Fig. 4*D*). In the presence of C9B7W, we found that MHCII- and FGL1-mediated LAG-3 CAR signaling was potently inhibited (Fig. 4*D*). Consistent with the previous report on C9B7W as a functional LAG-3 inhibitor (3), we also found C9B7W markedly blocks LAG-3 function in the DO11.10 T cell

assay (Fig. 4*E*). These data suggest that C9B7W is a D2-binding antibody which directly engages with the dimerization interface, impedes dimerization, and blocks LAG-3's T cell inhibitory function by disrupting ligand binding via avidity or allosteric effects.

Antibodies against D1 and D3 Can Also Affect LAG-3 Dimerization and Function. Given the heavy focus of D1 (particularly the MHCII-targeting loop 1 region) but not D2-targeted anti-LAG-3 antibodies in the current landscape for cancer immunotherapy (30), we sought to directly compare these two approaches, along with targeting the D3 domain, which shows proximity to the D2 dimerization interface (Fig. 1 *A* and *B*). We screened a set of hybridoma-generated mAbs against mouse LAG-3 with various binding epitopes, including D1 and D3, and similar affinities (*SI Appendix*, Fig. S10). We identified a D1-interacting antibody, M8-4-6, that was capable of binding to the non-Loop 1 region (*SI Appendix*, Fig. S10*A*). With our set of yeast-displayed alanine mutants, we further epitope mapped M8-4-6 to the tip of the D1 domain, where mutation of residues T146, R148, N151, and R152 to alanine resulted in a dramatic decrease in M8-4-6 binding signal (Fig. 5*A*). This region appears to be on the opposite face of D1 from loop 1 (i.e., purported MHCII binding site) and loop 2 [i.e., purported FGL1 binding site (10)]. Despite its binding at a distinct site away from loops 1 and 2, we found M8-4-6 also

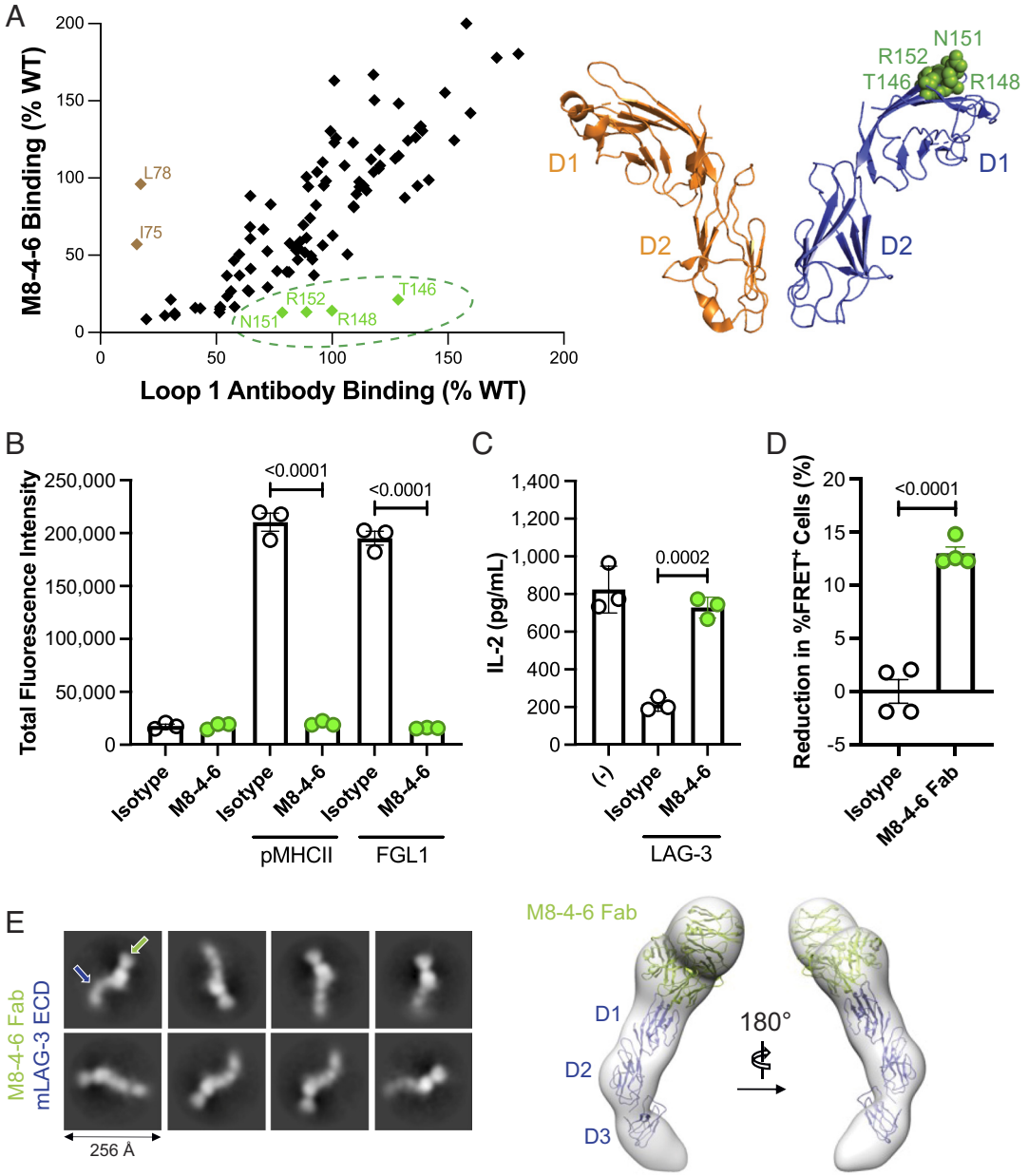

Fig. 5. M8-4-6 antibody binds to D1 tip, disrupts LAG-3 homodimerization, and potently blocks ligand binding. (*A*) Fine epitope mapping of D1 antibody (M8-4-6) by yeast surface display reveals a binding epitope at the tip of LAG-3 D1. LAG-3 residues important for M8-4-6 binding (T146, R148, N151, R152) are displayed as green spheres on the LAG-3 dimer. (*B*) LAG-3 CAR assay to evaluate LAG-3 ligand engagement in the presence of M8-4-6. Jurkat cells stably expressing a NFκB-GFP reporter and a LAG-3 CAR were co-cultured with 293T cells stably expressing pMHCII or transmembrane-fused FGL1. (*C*) IL-2 secretion to measure LAG-3-dependent T cell inhibition in the presence or absence of M8-4-6. DO11.10 cells expressing LAG-3 were co-cultured with LK35.2 cells pulsed with cognate peptide. Empty vector transduced T cells are represented by (−). (*D*) Flow-FRET data showing the effect of M8-4-6 Fab on LAG-3 dimerization. Reduction in %FRET$^+$ cells was calculated relative to the isotype. (*E*) Negative stain EM showing selected 2D class averages and the 3D map model of the M8-4-6 Fab with mouse LAG-3. The data in (*B*) and (*C*) are presented as the mean ± SEM and are representative of at least two independent experiments. All statistics were determined by Student's *t* test with *P* values noted in the figure.

demonstrated potent blocking capacity of LAG-3 binding to both pMHCII and FGL1 ligands in the LAG-3 CAR assay, as well as functional activity in the DO11.10 T cell assay (Fig. 5 *B* and *C* and *SI Appendix*, Figs. S11 and S12) (16). Given these results, we next tested whether M8-4-6 was similarly capable of disrupting LAG-3 cis-homodimerization. When the M8-4-6 Fab was tested in the flow-FRET assay with LAG-3-CFP- and LAG-3-YFP-expressing cells, we found that it could also disrupt LAG-3 dimerization (Fig. 5*D* and *SI Appendix*, Fig. S8 *A–D*), even though this antibody appears to bind to the tip of the LAG-3 D1 domain. Supporting this finding, we were also able to visualize dimer disruption by negative stain EM after co-complexation of the M8-4-6 Fab with mouse LAG-3 (Fig. 5*E*). Drawing a parallel to C9B7W, where LAG-3 dimerization appears to indirectly affect ligand binding, this finding may explain why M8-4-6 is able to block binding of both MHCII and FGL1 ligands, despite engagement via epitopes distinct from the ligands' purported binding sites on LAG-3 (10).

Given the proximity of the D3 domain to the dimer interface, we additionally tested a D3-targeted antibody, 410C9, for its ability to disrupt LAG-3 dimerization and ligand binding. Interestingly, a 410C9 Fab fragment was also shown to disrupt LAG-3 dimerization by EM analysis and flow-FRET (Fig. 6 *A* and *B*). Since we were not able to epitope map this D3-binding antibody with our yeast surface-displayed D1D2 alanine mutant library, we used AlphaFold-based prediction of 410C9 binding to the D3 domain to assist in positioning the Fab within our electron density map (Fig. 6*A*), which suggested that it binds at an interface close to the D2 domain. We next showed that like C9B7W and M8-4-6, the 410C9 antibody potently blocked ligand-dependent, LAG-3-mediated CAR signaling in a dose-dependent manner (Fig. 6*C* and *SI Appendix*, Figs. S12 and S13) and relieved LAG-3-mediated suppression in the DO11.10 T cell assay (Fig. 6*D* and *SI Appendix*, Fig. S12). Altogether, these data demonstrate that LAG-3 can be modulated by antibodies against domains beyond D2 that can lead to LAG-3 dimer disruption or altered LAG-3 geometries (*SI Appendix*, Fig. S12). In contrast to the major clinical focus on LAG-3 D1-targeted antibodies, these data clearly support the importance of D2 and D3 as promising epitopes for blocking LAG-3 inhibitory function.

Discussion

LAG-3 regulates T cell responses in the context of cancer and autoimmunity; however, the molecular mechanism and functional relevance of LAG-3 dimerization are currently unknown. In this study, we present the glycosylated murine LAG-3 homodimer structure at 3.78 Å and demonstrate the importance of cis-homodimerization in LAG-3 binding to both MHCII and FGL1 ligands and functional LAG-3 activity.

While previous reports had suggested that LAG-3 could be dimerizing through the D1 domain (9, 21), our structural analysis of the LAG-3 dimer revealed that two LAG-3 monomers interact through an extended interface, which mainly consists of the IgC D2 domain, in agreement with another recent structural study (10). This interface is mediated by a network of hydrogen bonds and hydrophobic interactions, which are important for the formation of a stable LAG-3 dimer. Furthermore, from our crystallographic analysis, we observed that positioning of the D1 domain by means of D2 homodimerization is dependent on the presence of N-linked glycans on residue N184. This finding implicates glycosylation in the formation and stability of the LAG-3 homodimer, adding to a growing number of studies highlighting the importance of glycosylation in mediating protein–protein interactions (31–33).

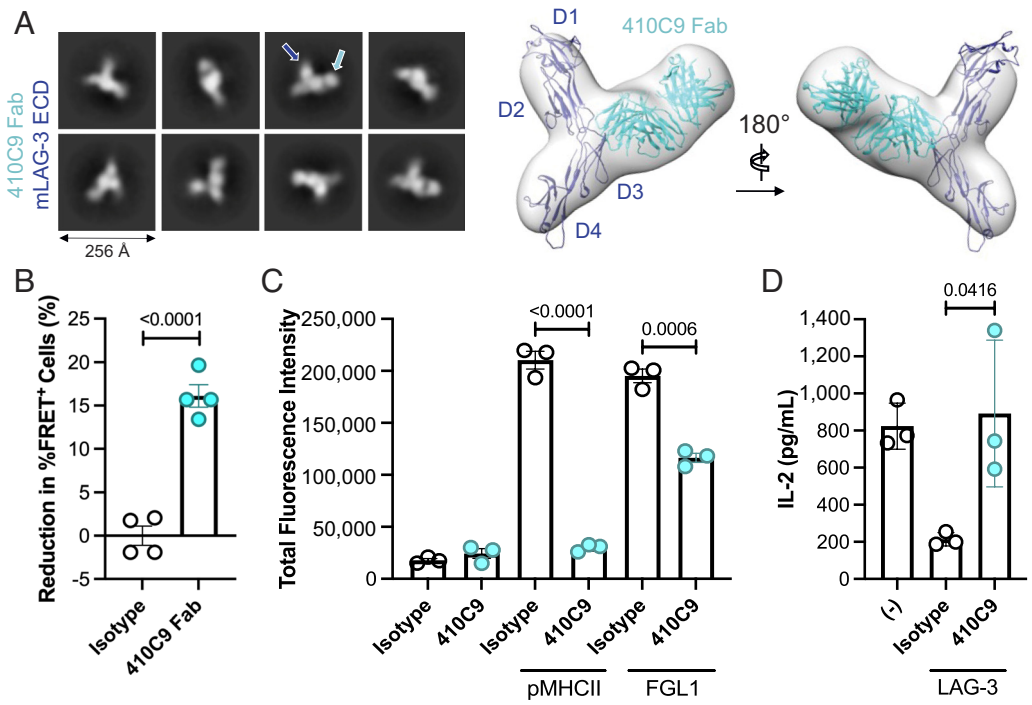

Fig. 6. 410C9 antibody disrupts LAG-3 dimerization and blocks ligand binding. (*A*) Negative stain EM showing selected 2D class averages and the 3D map model of the dimer-disrupting, 410C9 Fab with mouse LAG-3. (*B*) Flow-FRET data showing the effect of 410C9 Fab on LAG-3 dimerization. Reduction in %FRET$^+$ cells was calculated relative to the isotype. (*C*) LAG-3 CAR assay to evaluate LAG-3 ligand engagement in the presence of 410C9. Jurkat cells stably expressing a NFκB-GFP reporter and a LAG-3 CAR were co-cultured with 293T cells stably expressing pMHCII or transmembrane-fused FGL1. (*D*) IL-2 secretion to measure LAG-3-dependent T cell inhibition in the presence or absence of 410C9. DO11.10 cells expressing LAG-3 were co-cultured with LK35.2 cells pulsed with cognate peptide. Empty vector transduced T cells are represented by (−). The data in (*B*) and (*C*) are presented as the mean ± SEM and are representative of at least two independent experiments. All statistics were determined by Student's *t* test with *P* values noted in the figure.

To investigate LAG-3 dimer disruption as a means of modulating its activity, we introduced a hydrophobic-to-charge mutation at an evolutionarily conserved key residue in the dimer interface, W180, and showed that it reduced FRET-based dimerization, binding to MHCII and FGL1 ligands, and LAG-3 function, confirming the importance of the LAG-3 dimer interface in regulating its activity. Mutation of the N-linked glycosylation site N184 to glutamine resulted in a weaker disruption of dimerization in comparison to W180D. In turn, the N184Q mutation resulted in a weaker disruption of LAG-3-mediated ligand binding and function, further supporting that dimerization is strongly linked to ligand binding and function. Additionally, we showed that the murine LAG-3-binding C9B7W antibody, used in most animal tumor models to demonstrate therapeutic efficacy of LAG-3 modulation, binds to a hydrophobic patch in the LAG-3 D2 dimerization interface and potently inhibits ligand binding as measured by a sensitive LAG-3 CAR assay. Our data suggest that the C9B7W antibody interferes with the formation of LAG-3 homodimer by binding to the IgC domain of one of the monomers and sterically blocking dimer formation, which may in turn potentially inhibit ligand binding through allosteric and/or avidity effects. Although our study focused on MHCII and FGL1, homodimerization may also play a role in LAG-3 binding to other ligands, as C9B7W has been shown to block the LSECtin:LAG-3 and a-Synuclein:LAG-3 interactions (34, 35).

Intriguingly, our work showed that the M8-4-6 and 410C9 antibodies, which we propose target the LAG-3 D1 and D3 domains, respectively, are also capable of disrupting LAG-3 dimerization and ligand binding, which further highlights the complex nature of this signaling axis and suggests multiple potential approaches for inhibiting LAG-3 function. While these antibodies are not directly contacting the D2 dimerization interface residues or the proposed MHCII- and FGL1-ligand binding sites, it is possible that their binding to LAG-3 may result in conformational changes that disrupt dimerization, ligand binding, or both, and that LAG-3 association and ligand binding potentially go hand-in-hand to regulate the activity of this receptor.

In previous work, the D4-binding antibody F7 did not appear to disrupt dimerization in the crystal structure of human LAG-3, yet it also blocks LAG-3 function, as measured by NFAT reporter cell line (10). Interestingly, the F7 antibody enhanced LAG-3 binding to MHCII by surface plasmon resonance and was less effective at rescuing T cells from LAG-3-mediated inhibition than a D1-targeted antibody (10), indicating that future efforts to develop LAG-3 antagonists may benefit from measuring the ability of antibodies to disrupt dimerization. It is also possible that transmembrane domain-mediated interactions play a stronger role in D4-targeting antibodies, which are absent in the truncated LAG-3 ECD used in this work. This mechanism of LAG-3 signal blockade remains an area of active investigation.

A myriad of antibody programs that block the interaction of LAG-3 with MHCII are under clinical evaluation in cancer patients, including relatlimab (BMS), spartalizumab (Novartis), fianlimab (Regeneron), and others as reviewed recently (4), and have demonstrated some promising but modest signals in combination with anti-PD-1 (6). In particular, the fixed-dose combination of anti-LAG-3 relatlimab plus anti-PD-1 nivolumab (Opdivo) from Bristol Myers Squibb (BMS) was recently approved by the U.S. Food and Drug Administration given its role in improving progression-free survival over the anti-PD1 antibody nivolumab alone in melanoma (6); however, like other LAG-3 targeting mAbs, relatlimab shows little to no single agent activity in mouse tumor models (36, 37). To our knowledge, most antibodies under clinical development focus on blocking MHCII–LAG-3 interactions via binding the LAG-3 D1 domain. Given the importance of FGL1 ligand interactions (8, 38), as well as the role of the D2 dimerization interface on LAG-3 activity, clinical utilization of this biochemical pathway could potentially be expanded by broadening clinical exploration of the epitopes targeted beyond those focused on MHCII/LAG-3 blockade.

In conclusion, we have shown that LAG-3 homodimerization and glycosylation are critical for the formation of stable LAG-3 homodimer and its binding to MHCII and FGL1 ligands. Our findings provide a structural basis for the development of therapeutics that target LAG-3 dimerization, which may have implications for the treatment of cancer and autoimmune disease. While the focus of our study was on effector T cells, these findings may also be relevant to LAG-3's role on regulatory T cells and NK cells.

Materials and Methods

Protein Production and Purification. For structural studies, the LAG-3 ECD was cloned into the gWIZ vector with a C-terminal 6xHis tag. DNA was transiently transfected into Expi293F cells (ThermoFisher Scientific) using Expifectamine reagent (ThermoFisher Scientific). Five days post-transfection, supernatant was harvested, adjusted to pH 8.0, and sterile filtered. LAG-3 ECD was then purified using cobalt agarose resin (GoldBio) and concentrated in 25 mM Tris, 150 mM NaCl, pH 8.0 using Amicon Centrifugal Filters (Millipore Sigma, Burlington, MA). FGL1 was expressed and purified as previously described (8). Briefly, 293T cells were transfected with FGL1 containing an N-terminal 3xFLAG tag and purified with anti-FLAG M2 affinity resin (Sigma-Aldrich A2220). The affinity-purified protein was further purified by size exclusion chromatography to collect dimeric FGL1.

Antibody Production. LAG-3$^{-/-}$ mice were immunized with mouse and human LAG-3 Fc fusion protein in complete Freund's adjuvant and subsequently boosted twice with mouse and human LAG-3 Fc fusion protein in incomplete Freund's adjuvant as previously described (39). Hybridoma clones were obtained and characterized, two of which were utilized for this paper: M2-6-8 (Loop 1 binder) and M8-4-6 (D1, non-Loop 1 binder). The C9B7W and 410C9 hybridomas were kindly gifted by Dario Vignali. Antibody variable domain sequences from hybridomas producing mAbs against LAG-3 were obtained and then grafted onto mouse κ and IgG2a constant regions. L234A, L235A, and P329G mutations were introduced in the Fc region to disrupt effector function. The heavy and light chains for each antibody were expressed in Expi293F using a 1:2 mass ratio, respectively, and purified using Protein A (Cytiva). Fab fragments were produced by papain digestion as previously described (40). Briefly, cysteine-activated papain (Worthington) was incubated with purified C9B7W IgG at an appropriate ratio for 1 h at 37 °C. The reaction was quenched by adding 10 mM iodoacetamide. To isolate Fab from Fc and undigested IgG, the reaction mixture was passed through a Protein G column (GE Healthcare). Fab collected from flow-through was purified by size exclusion chromatography. To prepare complex samples, a twofold molar excess of Fab was incubated with LAG-3 for 1 h at room temperature.

X-Ray Crystallography Sample Preparation, Data Collection, and Structure Determination. LAG-3 ECD was concentrated to 7 mg/mL for the crystallization. Because of inherent diffraction issues, a large number of crystals were screened and several datasets were collected. The optimal crystals used for the successful structure solution had protein mixed with an equal amount of 0.1M Tris, 0.05M L-Arginine, 0.05M L-Glutamic acid monosodium salt hydrate, 14% PEG4000 at pH 8.1. Crystals were grown by sitting drop vapor diffusion at 16 °C and snap-frozen in mother liquor containing 10% MPD. Diffraction data were collected at Stanford Synchrotron Radiation Lightsource beamline 12-1. Datasets were indexed and scaled with XDS (41). The structure was solved by the Molecular Replacement method using various domains of the AlphaFold generated model (22, 23).

LAG-3 and LAG-3 Mutant Construction. LAG-3 cDNA fragments were amplified by PCR and cloned into a pCDH lentiviral expression vector (SystemBio #CD710B-1) under the EF1α-HTLV promoter using Gibson assembly. For FRET-related assays, LAG-3 fragments were cloned into pECFP and pEYFP plasmids (provided by Xiangpeng Kong). Mutants were constructed using site-directed mutagenesis and Gibson assembly.

Flow Cytometric FRET. Expi293F cells (ThermoFisher Scientific) were transfected with a CFP:YFP:PEI mass ratio of 0.5:0.5:3 in a 24-well plate at 37 °C in 8% CO_2. HEK293T cells were reverse transfected in a 96-well flat bottom plate with 300 ng total DNA. A 3:2 ratio of Lipofectamine 2000:DNA was used. Cells were analyzed after 48 h using a BD LSRII flow cytometer. Fab was incubated with cells at 1 μM on ice for at least 2 h and analyzed directly. The 407 nm violet laser was used to excite CFP and the 488 nm blue laser was used to excite YFP. CFP was detected using a 450/50 bandpass filter after excitation with the violet laser and YFP was detected using a 530/30 bandpass filter after excitation with the blue laser. FRET was detected using the 525/50 bandpass and 505 longpass filter after excitation with the violet laser.

Domain Epitope Mapping. Human embryonic kidney cell line 293T (ATCC, CRL-3216) was cultured in DMEM supplemented with 10% FBS, 2 mM L-Glutamine, 1X Penicillin/Streptomycin, 1 mM Sodium Pyruvate, and 20 mM HEPES. For domain epitope mapping of antibodies, HEK293T cells were reverse-transfected with LAG-3 truncations as described elsewhere (8). Hybridoma supernatant and 10 ng of goat anti-mouse IgG APC (Biolegend #Poly4053) were added 24 h after transfection and imaged using a CellInsight™ CX7 microscope (ThermoFisher).

Enzyme-Linked Immunosorbent Assays (ELISAs). Nunc MaxiSorp ELISA plates were coated with 5 μg/mL of mLAG-3 diluted in 50 μL PBS and incubated overnight at 4 °C. The plates were subsequently blocked with 400 μL ChonBlock ELISA Buffer (Chondrex, 9068) overnight at 4 °C, then bound for 3 h at 4 °C with varying concentrations of anti-LAG-3 antibodies diluted in 50 μL PBS + 1 mg/mL BSA + 0.1% Tween-20. Subsequently, 50 μL of a 1:7,500 dilution of HRP-labeled secondary antibody against mouse IgG (Jackson ImmunoResearch 715-035-150) was used for the detection of bound anti-LAG-3 antibodies, with colorimetric imaging occurring after incubation with 75 μL 1-Step Ultra TMB-ELISA Substrate Solution (ThermoFisher Scientific, 34028) quenched with 75 μL 2 M sulfuric acid. All steps prior to the addition of the TMB-ELISA Substrate Solution included a 3x wash with 400 μL PBS + 0.1% Tween-20.

Lentiviral Transduction of T Cells. 3A9 (ATCC #CRL-3293), DO11.10 (gift from Philippa Marrack), and Jurkat NFκB-GFP reporter cells (42) were maintained in RPMI 1640 supplemented with 10% FBS, 2 mM L-Glutamine, 1X Penicillin/Streptomycin, 1 mM Sodium Pyruvate, and 20 mM HEPES. Plasmids were reverse transfected into 293T cells to generate lentivirus. A pCDH:psPAX2:V-SVG DNA mass ratio of 2:1.5:1 and a Lipo2000:DNA ratio of 3:2 were used. After 16 h, the media was removed and replaced with T cell media. After an additional 24 h, viral supernatant was collected for transduction. Transduced cells were stained with anti-LAG-3 (410C9) and positively selected using a SY3200 Cell Sorter.

Flow Cytometry Immunostaining. To detect expression of LAG-3 on T cells, cells were incubated with 410C9 antibody (5 μg/mL), washed three times in FACS buffer, and stained with goat anti-mouse IgG APC (2 μg/mL, BioLegend #405308). For ligand binding, cells were stained with either I-A^b $OVA_{(323-339)}$ APC(1:10, MBL #TS-M710-2) or FGL1 (1 μg/mL) for at least 3 h on ice. After FGL1 binding, cells were washed three times in FACS buffer and further stained with anti-FLAG APC (1:100, Biolegend #637307). After staining, cells were washed three times in FACS buffer and analyzed on a BD™ LSR II flow cytometer.

IL-2 Assay and Quantitation. For DO11.10 T cell activation, $OVA_{(323-339)}$ peptide (Genscript #RP10610) was added to LK35.2 cells (ATCC #HB-98) at a concentration of 400 nM. The LK35.2-peptide mixture was added to a 384 well v-bottom plate at 1×10^4 cells. After 30 min, 2×10^4 DO11.10 cells were added per well for a final DO11.10:LK35.2 ratio of 2:1. For 3A9 T cell activation, 2×10^4 293T cells stably expressing I-A^k covalently bound to $HEL_{(48-62)}$ peptide were first added to a 384 well plate. Subsequently, 2×10^4 3A9 cells were added per well for a final 3A9:293T ratio of 1:1. After 20 to 24 h, the supernatant was collected and used for IL-2 quantitation by alphaLISA (Perkin Elmer #AL585C). For LAG-3 antibody blockade, anti-LAG-3 antibodies (50 nM) were incubated with the T cell hybridoma for 30 min at 37 °C, then added to the corresponding APC.

Jurkat LAG-3 CAR Assay. In each well of a 384 well plate, 1.2×10^4 293T cells stably expressing I-A^k HEL were added. LAG-3-CAR Jurkat NFκB-GFP cells were incubated with anti-LAG-3 or mouse IgG2a (BioXCell #BE0085) antibody for 30 min (50 nM) at 37 °C. The Jurkat–antibody mixture was then added at 2×10^4 cells per well. After 20 to 24 h, the plate was imaged using a CellInsight™ CX7 microscope. Images were quantified for total GFP fluorescence intensity using CellProfiler.

Negative Stain EM Imaging, Data Processing and Structural Modeling. For negative stain EM, a 3 μL aliquot of the complex sample at a concentration of 0.01 μg/μL was applied onto a glow-discharged carbon-coated grid (FCF400-CU, EM Sciences, EMS), blotted with filter paper (Whatman 1), and stained using 0.75% (w/v) uranyl formate (EMS) for 30 s. The images were collected on FEI Talos L120C TEM at 120 kV coupled with a Gatan OneView camera. Each image was acquired in a low-dose mode at magnification of 73,000x resulting in a pixel size of 2.0 Å, using a dose rate of ~40 $e^-/Å^2$. All single-particle processing, including particle picking, 2D classification, and 3D reconstruction, was performed using cryoSPARC v3.3.0 (43).

Yeast Surface Display. Domains 1 and 2 (D1D2) of the mouse LAG-3 ECD were cloned as a N-terminal fusion to Aga2 using an in-house developed vector called pPK, which contains Aga2p signal peptide and a cMyc tag between LAG-3 D1D2 and Aga2. Saccharomyces cerevisiae strain EBY100 was transformed with the pPK LAG-3 D1D2 vector and plated on SD-CAA plates for 3 d. Individual colonies were picked into SD-CAA liquid, grown overnight, and transferred to SG-CAA for 24 h of protein induction. For antibody binding, yeast were washed with PBSA (PBS with 0.1% BSA) and stained at 25 °C with chicken anti-cMyc (1:5,000, Invitrogen #A21281) and a dilution series of the mouse and rat anti-LAG-3 antibodies. After an additional wash, the yeast were stained at 4 °C with secondary antibodies: goat anti-chicken IgY H&L AF488 (1:1,000, Abcam #ab150169), goat anti-mouse IgG AF647 (for LAG-3 antibodies derived from mice, 1:1,000, Invitrogen #A21235), and goat anti-rat IgG AF647 (for the LAG-3 antibody derived from rats, 1:1,000, BioLegend #405416). The yeast were then washed once more before being analyzed on a BD Accuri™ C6 Flow Cytometer. Binding curves were made in GraphPad Prism using the geometric mean of the AF647 signal from $cMyc^+$ yeast, which enabled the approximation of each antibody's K_D. For epitope mapping studies, each mutant yeast clone was incubated with each antibody near that antibody's approximate K_D (at 300 pM).

Data, Materials, and Software Availability. Structure data have been deposited in PDB (8DGG) (24). All other data are included in the manuscript and/or *SI Appendix*.

ACKNOWLEDGMENTS. We thank members of the X.-P.K., J.W., and J.R.C. laboratories for helpful suggestions, Dario Vignali for providing the C9B7W and 410C9 hybridomas, Philippa Marrack for providing the DO11.10 T cell hybridoma, and Joseph Sall and Alice Feng-Xia Liang from the New York University Microscopy Core for their help with microscopy-related experiments. Use of the Stanford Synchrotron Radiation Lightsource, SLAC National Accelerator Laboratory, is supported by the U.S. Department of Energy, Office of Science, Office of Basic Energy Sciences under Contract No. DE-AC02-76SF00515. The Stanford Synchrotron Radiation Lightsource Structural Molecular Biology Program is supported by the Department of Energy Office of Biological and Environmental Research, and by the NIH, National Institute of General Medical Sciences (P30GM133894). The contents of this publication are solely the responsibility of the authors and do not necessarily represent the official views of National Institute of General Medical Sciences or NIH. The New York University Microscopy Core is partially supported by the New York University Cancer Center Support Grant NIH/NCI P30CA016087. The ThermoScientific CellInsight CX7 LZR was supported by the S10OD021727 grant. J.L.S. was funded by a graduate fellowship from the Stanford Bio-X Program and by a NIH 5 T32 AI007290 grant. J.D. is supported by a NIH/NIAMS T32 AR069515-07 grant (Translational Basic and Clinical Research Training in Rheumatology). J.A.F. was partially supported by an undergraduate fellowship from the Stanford Bio-X Program. Y.B.K. was funded by an Enhancing Diversity in Graduate Education Fellowship and an NSF Graduate Research Fellowship. Q.L. is the recipient of a Cancer Research Institute Irvington Postdoctoral Fellowship (CRI4179). P.L. was partially supported by the Stanford Molecular Biophysics Training Program NIH T32 Grant (T32GM136568). G.E.R. was funded by an NSF Graduate Research Fellowship and a Stanford Graduate Fellowship in Science & Engineering. J.W. is supported by the NIH (R01CA269898, R21AI163924-02),

Melanoma Research Alliance, the V Foundation, and the Mark Foundation. This work was supported by a young investigator award from the Melanoma Research Alliance (J.W.), a pilot award from the New York University Colton Center for autoimmunity (J.W.), an NIH R37CA273333-01 (J.W. and J.R.C.), and the Emerson Collective Cancer Research Fund (J.L.S. and J.R.C.).

Author affiliations: [a]Program in Immunology, Stanford University School of Medicine, Stanford, CA 94305; [b]Department of Bioengineering, Stanford University, Stanford, CA 94305; [c]Department of Pathology, New York University Grossman School of Medicine, New York, NY 10016; [d]Department of Biochemistry and Molecular Pharmacology, New York University Grossman School of Medicine, New York, NY 10016; [e]SLAC National Accelerator Laboratory, Stanford Synchrotron Radiation Lightsource, Menlo Park, CA 94025; [f]Department of Chemical Engineering, Stanford University, Stanford, CA 94305; [g]Program in Biophysics, Stanford University School of Medicine, Stanford, CA 94305; [h]Macromolecular Structure Knowledge Center, Stanford Sarafan ChEM-H Institute, Stanford, CA 94305; [i]Department of Molecular and Cellular Physiology, Stanford University School of Medicine, Stanford, CA 94305; and [j]The Laura and Isaac Perlmutter Cancer Center, New York University Langone Health, New York, NY 10016

Author contributions: J.L.S., J.D., K.-W.C., X.-P.K., J.W., and J.R.C. designed research; J.L.S., J.D., K.-W.C., J.A.F., I.I.M., Y.B.K., J.Y., Q.L., J.L., E.A.P., P.L., E.R., D.F., and G.E.R. performed research; J.L.S., J.D., K.-W.C., I.I.M., X.-P.K., J.W., and J.R.C. analyzed data; and J.L.S., J.D., J.W., and J.R.C. wrote the paper.

Competing interest statement: Authors are inventors on intellectual property related to this work that is owned by Stanford University and New York University. J.W. is on the Scientific Advisory Board of Rootpath Genomics and is a consultant for BMS (Relatlimab Advisory Council) and Beijing Hanmi Pharmaceutical Co., LTD. J.R.C. is a cofounder and equity holder of Combangio, Inc. (now Kala Bio), xCella Biosciences (now OmniAb), Charged Biotherapeutics, TwoStep Therapeutics, and Red Tree Venture Capital; has financial interests in Aravive, Inc.; is a member of the Board of Directors of OmniAb, Revel Pharmaceuticals, Excellergy Therapeutics, Rondo Therapeutics, Tachyon Therapeutics, and Biograph 55; and is a Board Observer at Acrigen Biosciences. The other authors have no competing interests.

1. D. M. Pardoll, The blockade of immune checkpoints in cancer immunotherapy. *Nat. Rev. Cancer* **12**, 252–264 (2012).
2. J. F. Grosso *et al.*, LAG-3 regulates CD8+ T cell accumulation and effector function in murine self- and tumor-tolerance systems. *J. Clin. Invest.* **117**, 3383–3392 (2007).
3. C. J. Workman, K. J. Dugger, D. A. A. Vignali, Cutting edge: Molecular analysis of the negative regulatory function of lymphocyte activation gene-31. *J. Immunol.* **169**, 5392–5395 (2002).
4. L. P. Andrews, A. E. Marciscano, C. G. Drake, D. A. A. Vignali, LAG3 (CD223) as a cancer immunotherapy target. *Immunol. Rev.* **276**, 80–96 (2017).
5. K. Richter, P. Agnellini, A. Oxenius, On the role of the inhibitory receptor LAG-3 in acute and chronic LCMV infection. *Int. Immunol.* **22**, 13–23 (2010).
6. H. A. Tawbi *et al.*, Relatlimab and nivolumab versus nivolumab in untreated advanced melanoma. *N. Engl. J. Med.* **386**, 24–34 (2022).
7. E. Baixeras *et al.*, Characterization of the lymphocyte activation gene 3-encoded protein. A new ligand for human leukocyte antigen class II antigens. *J. Exp. Med.* **176**, 327–337 (1992).
8. J. Wang *et al.*, Fibrinogen-like protein 1 is a major immune inhibitory ligand of LAG-3. *Cell* **176**, 334–347.e12 (2019).
9. B. Huard *et al.*, Characterization of the major histocompatibility complex class II binding site on LAG-3 protein. *Proc. Natl. Acad. Sci. U.S.A.* **94**, 5744–5749 (1997).
10. Q. Ming *et al.*, LAG3 ectodomain structure reveals functional interfaces for ligand and antibody recognition. *Nat. Immunol.* **23**, 1031–1041 (2022).
11. C. Guy *et al.*, LAG3 associates with TCR–CD3 complexes and suppresses signaling by driving co-receptor–Lck dissociation. *Nat. Immunol.* **23**, 757–767 (2022).
12. T. K. Maeda, D. Sugiura, I. Okazaki, T. Maruhashi, T. Okazaki, Atypical motifs in the cytoplasmic region of the inhibitory immune co-receptor LAG-3 inhibit T cell activation. *J. Biol. Chem.* **294**, 6017–6026 (2019).
13. C. J. Workman, D. S. Rice, K. J. Dugger, C. Kurschner, D. A. A. Vignali, Phenotypic analysis of the murine CD4-related glycoprotein, CD223 (LAG-3). *Eur. J. Immunol.* **32**, 2255–2263 (2002).
14. S. Cemerski *et al.*, T cell activation and anti-tumor efficacy of anti-LAG-3 antibodies is independent of LAG-3–MHCII blocking capacity. *J. Immunother. Cancer* **3**, P183 (2015).
15. K. L. Everett *et al.*, Generation of Fcabs targeting human and murine LAG-3 as building blocks for novel bispecific antibody therapeutics. *Methods* **154**, 60–69 (2019).
16. T. Maruhashi *et al.*, Binding of LAG-3 to stable peptide-MHC class II limits T cell function and suppresses autoimmunity and anti-cancer immunity. *Immunity* **55**, 912–924.e8 (2022).
17. M. Zettl *et al.*, Combination of two novel blocking antibodies, anti-PD-1 antibody ezabenlimab (BI 754091) and anti-LAG-3 antibody BI 754111, leads to increased immune cell responses. *Oncoimmunology* **11**, 2080328 (2022).
18. S.-R. Woo *et al.*, Immune inhibitory molecules LAG-3 and PD-1 synergistically regulate T-cell function to promote tumoral immune escape. *Cancer Res.* **72**, 917–927 (2012).
19. K. Thudium *et al.*, Preclinical characterization of relatlimab, a human LAG-3–Blocking antibody, alone or in combination with nivolumab. *Cancer Immunol. Res.* **10**, 1175–1189 (2022).
20. A. C. Anderson, N. Joller, V. K. Kuchroo, Lag-3, Tim-3, and TIGIT: Co-inhibitory receptors with specialized functions in immune regulation. *Immunity* **44**, 989–1004 (2016).
21. N. Li, C. J. Workman, S. M. Martin, D. A. A. Vignali, Biochemical analysis of the regulatory T cell protein lymphocyte activation gene-3 (LAG-3; CD223). *J. Immunol.* **173**, 6806–6812 (2004).
22. M. Varadi *et al.*, AlphaFold protein structure database: Massively expanding the structural coverage of protein-sequence space with high-accuracy models. *Nucleic Acids Res.* **50**, D439–D444 (2022).
23. J. Jumper *et al.*, Highly accurate protein structure prediction with AlphaFold. *Nature* **596**, 583–589 (2021).
24. J. L. Silberstein, I. I. Mathews, J. R. Cochran, Structure of glycosylated LAG-3 homodimer. RCSB PDB. https://www.rcsb.org/structure/8DGG. Deposited 23 June 2022.
25. D. Dong *et al.*, Structural basis of assembly of the human T cell receptor–CD3 complex. *Nature* **573**, 546–552 (2019).
26. L. Sušac *et al.*, Structure of a fully assembled tumor-specific T cell receptor ligated by pMHC. *Cell* **185**, 3201–3213.e19 (2022).
27. K. J. Laing *et al.*, Evolution of the CD4 family: Teleost fish possess two divergent forms of CD4 in addition to lymphocyte activation gene-31. *J. Immunol.* **177**, 3939–3951 (2006).
28. G. Chao, J. R. Cochran, K. D. Wittrup, Fine epitope mapping of anti-epidermal growth factor receptor antibodies through random mutagenesis and yeast surface display. *J. Mol. Biol.* **342**, 539–550 (2004).
29. G. Chao *et al.*, Isolating and engineering human antibodies using yeast surface display. *Nat. Protoc.* **1**, 755–768 (2006).
30. P. Agnihotri *et al.*, Epitope mapping of therapeutic antibodies targeting human LAG3. *J. Immunol.* **209**, 1586–1594 (2022).
31. Z. Meng, Z. Wang, B. Guo, W. Cao, H. Shen, TJC4, a differentiated anti-CD47 antibody with novel epitope and RBC sparing properties. *Blood* **134**, 4063 (2019).
32. L. Sun *et al.*, Targeting glycosylated PD-1 induces potent anti-tumor immunity. *Cancer Res.* **80**, 2298–2310 (2020).
33. C.-W. Li *et al.*, Eradication of triple-negative breast cancer cells by targeting glycosylated PD-L1. *Cancer Cell* **33**, 187–201.e10 (2018).
34. X. Mao *et al.*, Pathological α-synuclein transmission initiated by binding lymphocyte-activation gene 3. *Science* **353**, aah3374 (2016).
35. F. Xu *et al.*, LSECtin expressed on melanoma cells promotes tumor progression by inhibiting antitumor T-cell responses. *Cancer Res.* **74**, 3418–3428 (2014).
36. H. Li, X. Zhou, D. Li, V. Chromikova, Q. Lin, Abstract 2942: Improved LAG-3 humanized knock-in mouse model for assessment of mono- and combination therapy strategies for cancer treatment. *Cancer Res.* **81**, 2942 (2021).
37. E. Burova *et al.*, Preclinical development of the anti-LAG-3 antibody REGN3767: Characterization and activity in combination with the anti-PD-1 antibody cemiplimab in human PD-1xLAG-3–Knockin mice. *Mol. Cancer Ther.* **18**, 2051–2062 (2019).
38. K. Aigner-Radakovics *et al.*, The ligand-dependent suppression of TCR signaling by the immune checkpoint receptor LAG3 depends on the cytoplasmic RRFSALE motif. *Sci. Signal.* **16**, eadg2610 (2023).
39. Y. Chen *et al.*, Pik3ip1 is a negative immune regulator that inhibits antitumor T-cell immunity. *Clin. Cancer Res.* **25**, 6180–6194 (2019).
40. K.-W. Chan *et al.*, Structural comparison of human anti-HIV-1 gp120 V3 monoclonal antibodies of the same gene usage induced by vaccination and chronic infection. *J. Virol.* **92**, e00641-18 (2018).
41. W. Kabsch, XDS. *Acta Crystallogr. D Biol. Crystallogr.* **66**, 125–132 (2010).
42. J. Wang *et al.*, Siglec-15 as an immune suppressor and potential target for normalization cancer immunotherapy. *Nat. Med.* **25**, 656–666 (2019).
43. A. Punjani, J. L. Rubinstein, D. J. Fleet, M. A. Brubaker, cryoSPARC: Algorithms for rapid unsupervised cryo-EM structure determination. *Nat. Methods* **14**, 290–296 (2017).